A Microfluidic Investigation of the Synergistic Effect of Nanoparticles and Surfactants in Macro-Emulsion-Based Enhanced Oil Recovery

Ke Xu and **Peixi Zhu***, University of Texas at Austin; **Tatiana Colon,** Polytechnic University of Puerto Rico; and **Chun Huh** and **Matthew Balhoff,** University of Texas at Austin

Summary

Injecting oil-in-water (O/W) emulsions stabilized with nanoparticles (NPs) or surfactants is a promising option for enhanced oil recovery (EOR) in harsh-condition reservoirs. Stability and rheology of the flowing emulsion in porous media are key factors for the effectiveness of the EOR method. The objective of this study is to use microfluidics to (1) quantitatively evaluate the synergistic effect of surfactants and NPs on emulsion dynamic stability and how NPs affect the emulsion properties, and to (2) investigate how emulsion properties affect the sweep performance in emulsion flooding.

A microfluidic device with well-defined channel geometry of a high-permeability pathway and multiple parallel low-permeability pathways was created to represent a fracture–matrix dual-permeability system. Measurement of droplet coalescence frequency during flow is used to quantify the dynamic stability of emulsions. An NP aqueous suspension (2 wt%) shows excellent ability to stabilize the macro-emulsion when mixed with a trace amount of surfactant (0.05 wt%), revealing a synergistic effect between NPs and surfactant.

For a stable emulsion, when a pore throat is present in the high-permeability pathway, it was observed that flowing emulsion droplets compress each other and then block the high-permeability pathway at a throat structure, which forces the wetting phase into low-permeability pathways. Droplet size shows little correlation with this blocking effect. Water content was observed to be much higher in the low-permeability pathways than in the high-permeability pathways, indicating different emulsion texture and viscosity in channels of different sizes. Consequently, the assumption of bulk emulsion viscosity in the porous medium is not applicable in the description and modeling of the emulsion-flooding process.

Flow of emulsions stabilized by an NP/surfactant mixture shows droplet packing in high-permeability regions that is denser than those stabilized by surfactant only, at high-permeability regions, which is attributed to the enhanced interaction between droplets caused by NPs in the thin liquid film between neighboring oil/water (O/W) interfaces. This effect is shown to enhance the performance of emulsion-blockage effect for sweep-efficiency improvement, showing the advantage of NPs as an emulsion stabilizer during an emulsion-based EOR process.

Introduction

Among all EOR options, the use of macro-emulsion as displacement fluid (emulsion flooding), especially for heavy-oil recovery (Mendoza et al. 1991), has so far received limited attention (Islam and Ali 1989; Mandal et al. 2010b) despite its good potential (Rocha de Farias et al. 2012; Karambeigi et al. 2015). A major potential advantage of emulsion-based EOR is that the emulsion blocks the high-permeability paths and then forces more displacing fluid into low-permeability regions, which is difficult to achieve with a single-phase displacing fluid (Alvarado and Marsden Jr. 1979; Thomas and Farouq Ali 1989; Cobos et al. 2009; Romero et al. 2011; Pei et al. 2015). Therefore, this EOR method is particularly promising for highly heterogeneous and naturally fractured reservoirs. Properties of emulsion flow are highly dependent on droplet size, droplet-size distribution, phase ratio, and rheology of both the continuous and the dispersed phase (Thomas and Farouq Ali 1989; Tadros 1994). Even for a given emulsion system, its effective bulk viscosity might be quite different in channels/pores of different length scales. McAuliffe (1973) found from coreflood experiments that O/W emulsion proportionally reduced the permeability in high-permeability cores more than in cores of lower permeability. They proposed that the most-effective emulsion to enhance oil recovery is one in which the droplet diameters are slightly larger than the pore-throat constriction in the high-permeability zone. However, a fundamental understanding of such diversion mechanisms of emulsion flow in porous media may require visualization of in-situ flow at the pore scale, which is not feasible with corefloods.

Microfluidics provides a platform to directly visualize multiphase flow in micron-scale geometries. With advanced fluid-control theory/techniques (Abgrall and Gué 2007), as well as the reproducible and proven technologies to manufacture microfluidic chips with complicated channel geometries (Stone et al. 2004; Song et al. 2014), microfluidics is now widely applied in chemical processes (Song and Ismagilov 2003), material synthesis (Xu et al. 2012), and biological and chemical analyses (Martinez et al. 2010; Nilghaz et al. 2012). In porous media, two- or three-phase flow occurs within pores and throats of length scales of microns. Microfluidics thus allows detailed observation of immiscible fluid-displacement processes that occur in porous media at the pore scale. In the past decade, breakthroughs have been made on the quantification of fundamental flow phenomena in porous media, including single-phase flow (Koo and Kleinstreuer 2003), multiphase flow (Xu et al. 2006), interfacial phenomena (Lee et al. 2015), and emulsion behavior (Shah et al. 2008; Xu et al. 2015a). Multiphase flow in specialized geometries, such as pore throats, which is key in understanding EOR mechanisms, has also been studied (Wang et al. 2014; Xu et al. 2015b). Furthermore, the immiscible-displacement processes for improved-oil-recovery applications, such as waterflooding (Chang et al. 2009), foam flooding (Ma et al. 2012), and polymer/surfactant flooding (Aktas et al. 2008; Chang et al. 2009), have also been investigated with 2D microfluidic porous networks (micromodels).

Microfluidics has been used in investigation of flow in fracture/matrix dual-permeability porous media, in which emulsion-based EOR is claimed to have advantages in blocking high-permeability pathways and then diverting the displacing fluid into low-permeability paths (Cobos et al. 2009; Mandal et al. 2010a). Wan et al. (1996) first investigated single-phase flow in fractured porous media with a glass micromodel, and directly showed the fracture and flow velocity profile. Multiphase problems such as

* Corresponding author; email: zpeixi@utexas.edu

This paper (SPE 179691) was accepted for presentation at the SPE Improved Oil Recovery Conference, Tulsa, 11–13 April 2016, and revised for publication. Original manuscript received for review 25 January 2016. Revised manuscript received for review 28 July 2016. Paper peer approved 2 August 2016.

gas-in-water flow in dual-permeability networks represented by micromodels have also been addressed. Zhang et al. (2011) applied a micromodel to investigate supercritical carbon dioxide (CO_2) displacement of water in a fractured matrix. They found that, if only CO_2 was injected, the fingering effect in a dual-permeability geometry is not preventable, but if water was injected together with CO_2, the fingering effect disappeared. In particular, research on foam flooding in microfluidics has been reported for dual-permeability geometries. Ma et al. (2012) first constructed 2D glass micromodels to investigate foam flow in dual-permeability porous media, and showed a higher sweep efficiency of foam flooding than gas flooding. Conn et al. (2014) investigated foam flooding in a tripermeability micromodel that consisted of a fracture, high-permeability network, and low-permeability network, and found that foam flooding showed higher sweep efficiency than gas flooding and water-alternating-gas flooding. Because foam flooding and emulsion flooding share many similarities in basic flow principles, the results of foam flooding in dual-permeability porous media are encouraging for emulsion-based EOR. However, those results of foam EOR may not directly translate to emulsion flooding, because of the much-lower compressibility and interfacial tension (IFT) in an emulsion system than in a foam system, which can have a big impact on the flow dynamics. Although some microfluidic research on emulsion flooding has been performed and its potential on mobility control was proposed (Cobos et al. 2009), there is still no microfluidic-based direct observation of emulsion flow in dual-permeability porous media. In this work, we conducted microfluidic experiments to study emulsion behavior with a geometry representative of fracture/matrix dual-permeability and discuss the effect of emulsion on sweep efficiency.

Stability of emulsion droplets is one of the most-important factors in the effectiveness of oil recovery in emulsion-based EOR. Emulsions are typically stabilized by surface-active agents, with their ability to help generate dispersions by reducing IFT and to delay/prevent droplet coalescence (Garrett 1965). Polymers can also be applied as a stabilizer by increasing the continuous-phase viscosity and forming a chain-network between droplets, which can prevent droplet coalescence (Tadros 1994). However, the application of both surfactant and polymer in high-temperature and/or high-salinity subsurface conditions is often difficult because they become chemically degraded or they lose their surface activity.

NPs have been proposed as a good emulsion stabilizer in many fields including EOR (Hashemi et al. 2014; Bennetzen and Mogensen 2014). They are known to possess excellent physical and chemical stability in harsh subsurface conditions (Ryles 1988; Yu and Xie 2012; Metin et al. 2013). In an O/W system, NPs can adsorb on the fluid/fluid interface (Aktas et al. 2008; Du et al. 2010; Okada et al. 2012; Bhattacharya and Basu 2013), which can lead to generation/stabilization of emulsion/foam (Hunter et al. 2008; Chevalier and Bolzinger 2013; Nallamilli et al. 2014), because of the reduction of IFT (Du et al. 2010; Rana et al. 2012; Bizmark et al. 2014), the electrostatic and steric repulsion (Pickering 1907), and the change of emulsion rheology (Ravera et al. 2008; Sagis 2011; Schmitt et al. 2014). Thus, NPs have attracted attention for foam or emulsion-based EOR (Mandal et al. 2010a; Bennetzen and Mogensen 2014). Espinoza et al. (2010) showed the improvement of oil recovery over waterflooding when NP-stabilized CO_2 foam was used as the displacing phase. Sharma et al. (2015) tested the EOR potential for NP-stabilized emulsion along with viscous aqueous phase and showed improvement in cumulative oil recovery by 5%. It should be noted that NPs are only likely to be relevant for field applications if the price is significantly cheaper than surfactant, or the consumption can be significantly reduced.

It has been reported that the use of NPs and surfactant together can lead to further improvement in reducing IFT and stabilizing emulsions (Binks et al. 2007, 2008; Chevalier and Bolzinger 2013; Worthen et al. 2013). Binks et al. (2007) showed a synergistic effect of NP/surfactant mixture that enhanced emulsion stability. They found that the addition of surfactant makes the NP more hydrophobic, thus increasing NP adsorption on the O/W interface. Pei et al. (2015) found that a combination of NPs and surfactant could increase the bulk viscosity of emulsion and then provide a better oil recovery. Taking advantage of the NP/surfactant mixture may result in a more cost-effective and efficient emulsion-stabilization agent.

In this work, with the help of microfluidic experiments, we attempt to provide an explanation to the following problems: (1) emulsion distribution and oil-saturation distribution during emulsion flooding in the fracture and matrix; (2) displacement performance difference of NP-stabilized emulsion from surfactant-stabilized emulsion in this geometry; and (3) the effect of droplet size and injection-phase ratio on the flow and on local oil saturation.

Methods

Materials. In our microfluidic experiments, decane was used as the oil phase, and deionized (DI) water with or without additives (NPs, surfactant, or their combination) was used as the aqueous phase. The silica NPs used are highly hydrophilic and have an average size of 5 nm (Xu et al. 2015b). The NPs are provided as a 20 wt% aqueous dispersion and were diluted to achieve the desired concentration (2 wt%). The surfactant used is polyoxyethylenesorbitan monopalmitate (Tween 40), a water-soluble nonionic surfactant.

Glass was used as the microfluidic material. The chip fabrication followed a standard lithography process and hydrofluoric acid (HF) etching (Gravesen et al. 1993). Channels of specified depth were obtained by controlling the HF-etching time. The etched glass piece was bonded to a cover piece by heating at 690°C for 1 hour. After being immersed into NaOH solution for 5 hours, the wettability is surmised, although not confirmed, to be completely water-wet (Xu et al. 2014).

Micromodel Design for Fracture/Matrix Porous Media. A typical natural fracture/matrix porous medium is shown in **Fig. 1a.** To simulate flow in a characteristic geometrical structure, we designed the 2D microfluidic chip shown in Fig. 1b. The channel assembly is divided into two parts in sequence.

Part I. Emulsion generator that can produce emulsions with controllable droplet size, droplet frequency, and total liquid-flow rate, as shown in the top part of Fig. 1b and Fig. 1c. A T-junction for creating monodispersed O/W emulsion droplets (Fu et al. 2011) was set upstream of the microfluidic device. The size and generation frequency of the droplets are controlled by adjusting the injection rates of the aqueous ("aqueous-phase inlet" shown in Fig. 1b) and oil phases ("oil inlet" shown in Fig. 1b) (Xu et al. 2006). The channel is then widened in the downstream of the T-junction, where another aqueous-phase injection inlet (aqueous-phase Inlet 2 shown in Fig. 1b) exists to control the total flow rate.

Part II. Dual-permeability geometry to represent fracture–matrix porous media, as shown in the bottom part of Fig. 1b and Figs. 1d and 1e. A high-permeability path with a width of 617 µm (marked as main channel) opens to several diverging low-permeability side paths of different widths from 27 to 67 µm, as shown in Fig. 1d and Fig. 1e. A throat with a narrow width of 67 µm (marked as main throat) is set in the main channel downstream of all side paths, as shown in Fig. 1f. The main-channel length (not shown in the figures) from the emulsion generator to the main throat is approximately 4.5 mm. All side paths merge with the main channel at the downstream of the main throat. The cross section of all channels is flat-rectangular, and the geometry parameters are listed in **Table 1.** The experimental platform is shown in Fig. 1g.

It should be noted that, because the low-permeability pathways have a depth of 17 µm and a width from 27 to 67 µm, the characteristic dimension of those channels would be from 19 to 24 µm $\left(\sqrt[4]{\text{width} \times \text{depth}^3}\right)$, which is typical of high-permeability

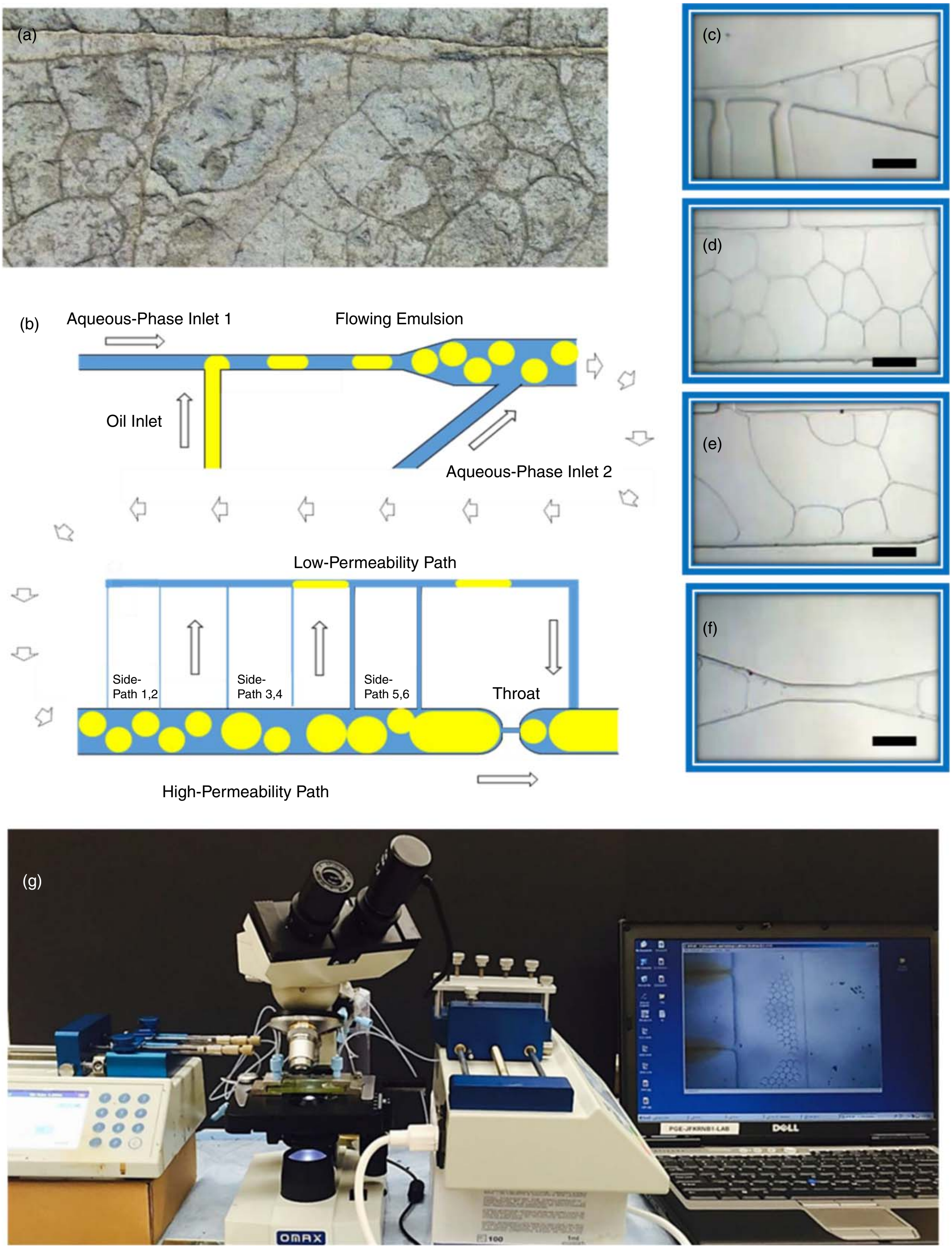

Fig. 1—(a) Image of a typical dual-permeability porous medium showing a complex of natural fractures and matrix [image courtesy of Jessica M. Winder (https://natureinfocus.wordpress.com/) with permission]; (b) the schematic of the microfluidic design. An emulsion generator (top part) is in the upstream where emulsion with controllable droplet size, flux ratio, and total flux is generated; a dual-permeability geometry is in the downstream, where a throat (main throat) is set in the high-permeability channel (main channel). There are several low-permeability side paths set along the main channel, which run across the throat and merge with the main channel again at the downstream of the main throat. (c)–(f) Microscopic images for emulsion flow along the main channel, from (c) the emulsion generator through side-path entrances (d) and (e), to the main throat (f). The scale bars in (c)–(f) represent 200 μm. (g) The experiment platform that consists of several pumps, a microscope with a camera, a computer, and the microfluidic chip (micromodel).

Channel	Width (μm)	Depth (μm)
Aqueous-Phase Inlet 1	47	17
Aqueous-Phase Inlet 2	35	17
Oil Inlet	47	17
Main Channel	617	17
Main Throat	67	17
Side Path 1,2	27	17
Side Path 3,4	37	17
Side Path 5,6	67	17

Table 1—Channel dimensions in the microfluidic device.

sandstone reservoirs, such as Bentheimer sandstone (Al-Yaseri et al. 2015). In the flow experiments, the total flow rates were controlled between 25 and 30 μL/h. Assuming a typical porosity of 0.2, the Darcy velocity of the emulsion in the high-permeability pathway (much like the fractures in sandstone reservoirs) is between 37 and 45 ft/D. Because the width of low-permeability pathways is one order of magnitude smaller, and their lengths are the same order of magnitude as the high-permeability pathway, under this pressure gradient, the characteristic flow in those channels would be on the order of 1 ft/D, within the range of typical flow rate in the matrix of sandstone reservoirs.

Experiment Operation and Emulsion-Stability Test. As shown in Fig. 1c, monodispersed oil droplets were generated from the emulsion generator, and then flowed downstream into the dual-permeability geometry. All images and videos were captured after the flow reached steady state (i.e., when droplet-generation frequency and droplet sizes showed no change with time and the passing of droplets through the main throat was of constant frequency).

Emulsion stability is an important factor in emulsion-flooding processes. The decrease in volume fraction of emulsion layer under gravity force in a quiescent state with time is a good preliminary way to quantify the emulsion stability. However, it is well-documented that the method has major shortcomings in this study (Binks et al. 2007). For realistic representation of dynamic stability of emulsions at reservoir flowing conditions, a better measurement approach is required, especially to evaluate effectiveness of emulsion stabilizers for EOR applications. At least two factors may affect the stability of emulsion flowing in porous media: (1) liquid/solid surface interactions, which are significant in porous media because of confined spaces at the micron scale, and (2) much-larger asymmetric compressive stress on droplets (Boyd et al. 1972) driven by a shearing force of the continuous phase, both of which are absent in the quiescent method.

An improved measurement of emulsion stability, which is more representative of in-situ reservoir conditions, can be easily achieved in our microfluidic design: From the captured videos of emulsion flow along the 4.5-mm-long main channel, the coalescence strength can be measured by "counting" the change of droplet diameter when the flow is steady state.

Image Processing and Data Analysis. All data were captured when the emulsion flow was at steady state. The 2D images of the flowing emulsion in the microchannel were captured by a digital camera connected to the microscope. Because of the difference in refractive indices between the oil and aqueous phases, the edges of oil droplets were clearly identified and recorded. Then the images were converted into a binary format with oil phase in black and water phase in white. A Matlab program was created to count the black and white pixel ratio to calculate the area fraction of the oil phase in the channel. Because the depth of the channel is much less than the width and the droplet diameter, droplets are in the form of circular disks. Therefore, the 2D area fraction of oil droplets was assumed equal to the volume fraction of the oil phase; and further, this oil volume fraction is defined as the local "oil saturation" for the microchannel system.

Results and Discussion

Description of Emulsion Flow Behavior in Fracture/Matrix Micromodel. When the flow in the main channel meets a side path, the flow diverges, and some fluid flows into the low-permeability channel. For all divergences, more water than oil flows into the side paths because of capillary resistance. If the emulsion was not stable enough, coalescence could be observed along the main channel, as shown in Figs. 1d and 1e.

It is noticeable that the volume fraction of oil phase in the channel is much larger than its flux fraction, which indicates that the velocity of the aqueous phase is considerably larger than that of the oil phase, mainly because of the existence of the main throat, where oil droplets were slowed down by capillary forces. Upstream of the main throat, oil droplets have close contact with each other and experience deformation until they pass the main throat.

Dynamic Stability of O/W Emulsion With Different Stabilizers. The total flow rate was maintained at 30 μL/h, oil injection rate at 10 μL/h, and the droplet diameter at approximately 190 to 210 μm. It was observed that an oil droplet needed approximately 14 to 16 seconds to reach the throat from the time of generation. Four stabilizing systems were tested in the experiment: (1) 2 wt% surfactant, (2) 2 wt% NPs, (3) trace amount of surfactant (0.05 wt%), and (4) a combination of 2 wt% NPs and 0.05 wt% surfactant.

The quantitative results of the test are provided in **Fig. 2a.** In the plot of average droplet size vs. flowing distance, a larger slope indicates more frequent coalescence. For the two surfactant-only systems, we found that 0.05 wt% surfactant (purple curve) cannot maintain a very stable emulsion, whereas 2 wt% surfactant (green curve) can. For the two NP systems, 2 wt% NPs alone (red curve) could barely prevent the droplets from coalescing, the stabilizing effect of which is even poorer than 0.05 wt% surfactant; however, when 0.05 wt% surfactant was mixed with 2 wt% NPs in the aqueous phase (blue curve), the stability of emulsion was substantially improved and became as good as the 2 wt% surfactant.

Images of flowing emulsion at the emulsion generator and before the main throat are shown for the 2 wt% NP case (Fig. 2b and Fig. 2c, respectively) and the combination case of 2 wt% NPs and 0.05 wt% surfactant (Fig. 2d and Fig. 2e, respectively). The images allow visualization of how emulsion stability can affect the droplet size.

We conclude from the previous results that trace amounts of surfactant improve the NP performance in stabilizing emulsions. This indicates that surfactant plays a very important role in enhancing the adsorption of NPs from the aqueous phase onto the O/W interface. This synergistic effect could be attributed to the surfactant's effect to make silica NPs more hydrophobic (Binks et al. 2007; Chevalier and Bolzinger 2013). Continued analysis is focused on the two most-effective stabilizers: 2 wt% Tween 40, marked as "SF," and a combination of 2 wt% NPs with 0.05 wt% Tween 40, marked as "NP/SF". The water/oil IFT was found to be similar for the two stabilizers (9.8 and 9.1 mN/m for SF and NP/SF, respectively) according to a pendant-drop experiment.

Local Oil Saturations Along the High-Permeability Channel. Because of the entrance capillary pressure, it is easier for water than oil to imbibe into the low-permeability side paths. As a consequence, the volume fraction of oil increases with each passing of a side path. No oil droplets were observed to enter the 27- and 37-μm side paths in our experiments, but some could enter the 67-μm side paths, which have the same dimensions as the main throat and thus similar capillary forces. When the flow reached steady state, the oil volume fraction (local oil saturation) reached its maximum just upstream of the main throat. We refer to the local

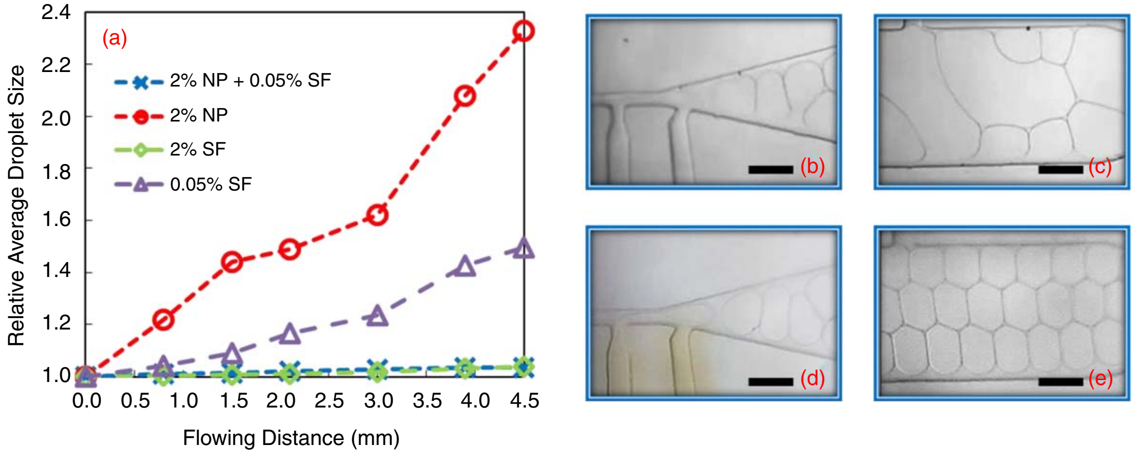

Fig. 2—(a) Relative average droplet size vs. flow distance of emulsion along the main channel for four different emulsion-stabilizing systems. Blue crosses represent 2 wt% NPs mixed with 0.05 wt% Tween 40; red circles represent 2 wt% NPs; green diamonds represent 2 wt% Tween 40; purple triangles represent 0.05 wt% Tween 40. (b)(c) Images of droplets stabilized by 2 wt% NPs, at the emulsion generator and before the main throat, respectively. (d)(e) Images of droplets stabilized by 2 wt% NPs combined with 0.05 wt% Tween 40, at the emulsion generator and before the main throat, respectively. The scale bars in (b)–(e) represent 200 µm.

oil saturation in the main channel just downstream of the emulsion generator as 'average oil saturation (S_{oa})," and refer to the local oil saturation downstream of all divergences and upstream of the main throat as "maximum oil saturation (S_{om})."

S_{oa} and S_{om} are important parameters of this work; analysis can provide a deeper understanding of the emulsion fluidic behavior. The difference between S_{oa} and injection flow ratio could help to describe the velocity difference of the two phases. The comparison between S_{oa} and S_{om} may indicate the difference of emulsion texture in the main channel and in the side paths. The S_{om} is also a good indicator of how well the droplets block the high-permeability path: For fixed IFT, larger S_{om} indicates better blockage of the high-permeability path, which can force more liquid into low-permeability paths.

Fig. 3 shows the difference of S_{oa} and S_{om}. At the beginning of the main channel where the oil droplets are generated, droplets flow without much compression from their neighbors. After all divergence channels and right before the main throat, droplets are blocked by the throat and become crowded, deform, and water is forced to flow through the very narrow gap at the two sides of the main channel.

S_{oa} and S_{om} were calculated at the fixed total flux of 26 µL/h for different droplet sizes. The results from two O/W injection fractions (0.192 and 0.385, corresponding to oil-injection rates of 5 and 10 µL/h, respectively) and two stabilizing systems (SF, NP/SF) are compared in **Fig. 4.** Here, we found that S_{om} is generally 10 to 20% higher than S_{oa}, and both are considerably larger than the corresponding oil-injection fraction, indicating a much larger

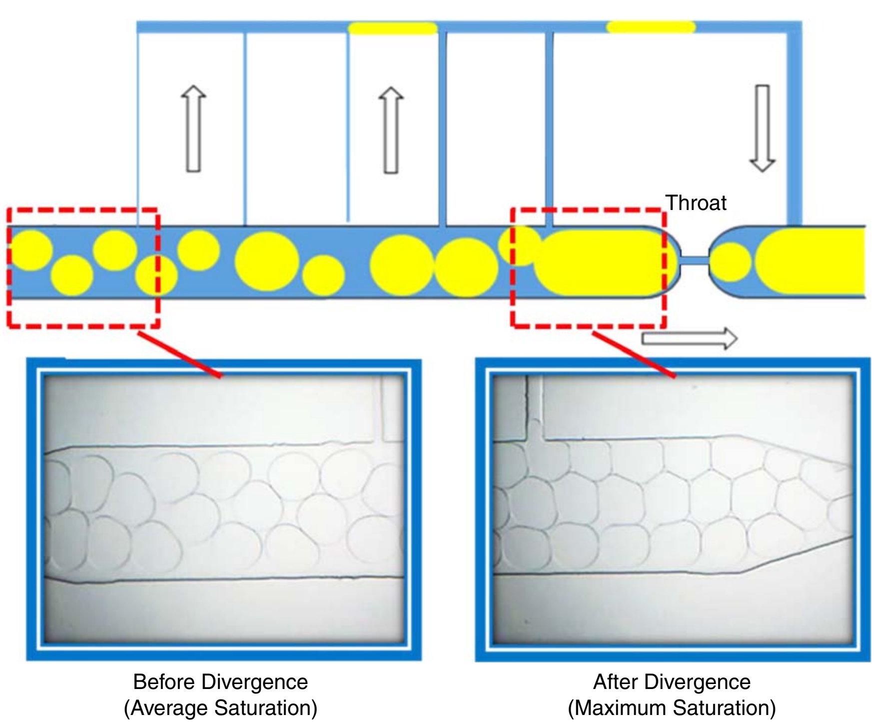

Fig. 3—Two observation locations for local oil-saturation comparison: The upstream part of the main channel before meeting any side paths (before divergence), where the oil saturation is marked as "average saturation" S_{oa}; the part of the main channel right before the main throat and after all side paths (after divergence), where the oil saturation reaches its maximum for a given system, marked as "maximum saturation" S_{om}.

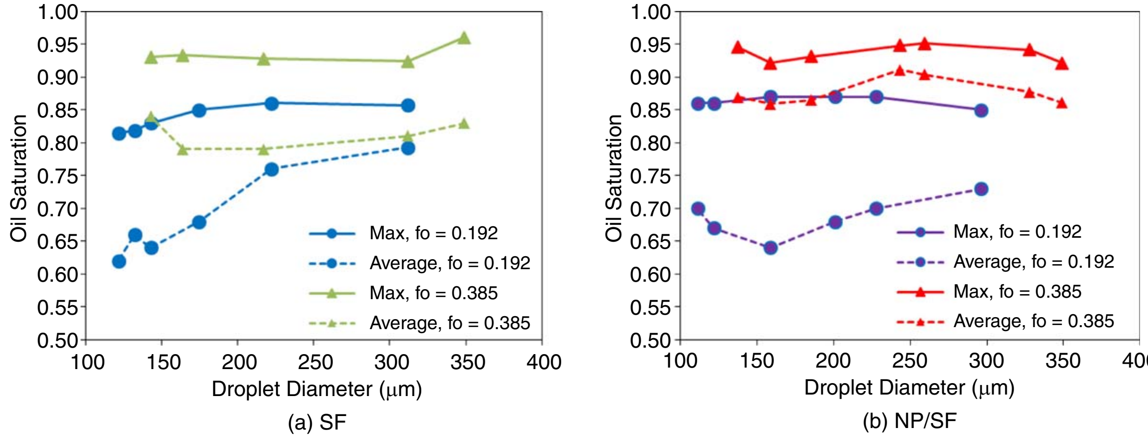

Fig. 4—S_{oa} and S_{om} vs. oil-droplet diameters at fixed total emulsion flux of 26 μL/h when applying (a) 2 wt% Tween 40 or (b) 2 wt% NPs mixed with 0.05 wt% Tween 40 as emulsion stabilizer. Circles represent oil saturation when oil flux is 5 μL/h and water flux is 21 μL/h (i.e., the fractional flow of oil is 0.192); triangles represent oil saturation when oil flux is 10 μL/h and water flux is 16 μL/h (i.e., the fractional flow of oil is 0.385). Solid line represents the maximum oil saturation S_{om} (i.e., the local oil saturation in the main channel after divergence and before main throat); dotted line represents the average oil saturation (i.e., the local oil saturation when droplets are just generated, before flowing through any side paths).

relative permeability of water than of oil in this geometry. When increasing the oil-injection ratio, both S_{oa} and S_{om} increase. These trends were observed in both SF and NP/SF systems.

The S_{oa} data do not show clear trends when plotted against droplet diameter, as shown in Fig. 4. It may be attributed to the randomness of droplet movement upstream of the main channel because of infrequent interaction among free oil droplets, as well as the pressure fluctuation corresponding to trapping and mobilization of oil droplets at the main throat. As a result, further discussion is only based on S_{om}, the data of which are consistent.

Remarkably, S_{om} remains almost constant for different droplet sizes in all parallel experiments. We propose that the accumulation of droplets before the main throat is controlled by the balance of shear force and capillary pressure. Thus, if the droplet size is considerably larger than the throat size, then both the shear rate and the capillary force would be similar and not related to the droplet size.

We also obtained the S_{om} when the total injection rate is 30 μL/h and the oil-injection rate is 20 μL/h, as shown in **Fig. 5.** Similar to findings in previous experiments, only small changes in S_{om} were observed when the droplet diameter changed from 100 to 400 μm, for both SF and NP/SF systems.

Flow-Divergence Quantification and Potential Thickening Effect on Sweep Efficiency. The "emulsion-blockage" effect is a commonly cited reason for emulsion flooding improving oil recovery (Islam and Ali 1989; Mendoza et al. 1991; Mandal et al. 2010b). We have shown that the increase of oil-injection fraction can increase the local oil saturation at the main throat, which indicates an enhancement in emulsion blockage in the high-permeability pathway. Here, we quantitatively show how the change in blockage effect can affect the flow into low-permeability regions.

As shown in the channel geometry (Fig. 1b), the high-permeability pathway and the low-permeability pathways merge downstream of the main throat, which leads to a sudden change of flow rate in the main channel before and after the merge. As a consequence, the droplet's velocity in the main channel after the merge, denoted as v_2, should be larger than that before the merge, denoted as v_1. The v_1 and v_2 are calculated by tracking a droplet's moving distance during a certain time period, as shown in **Fig. 6a and**

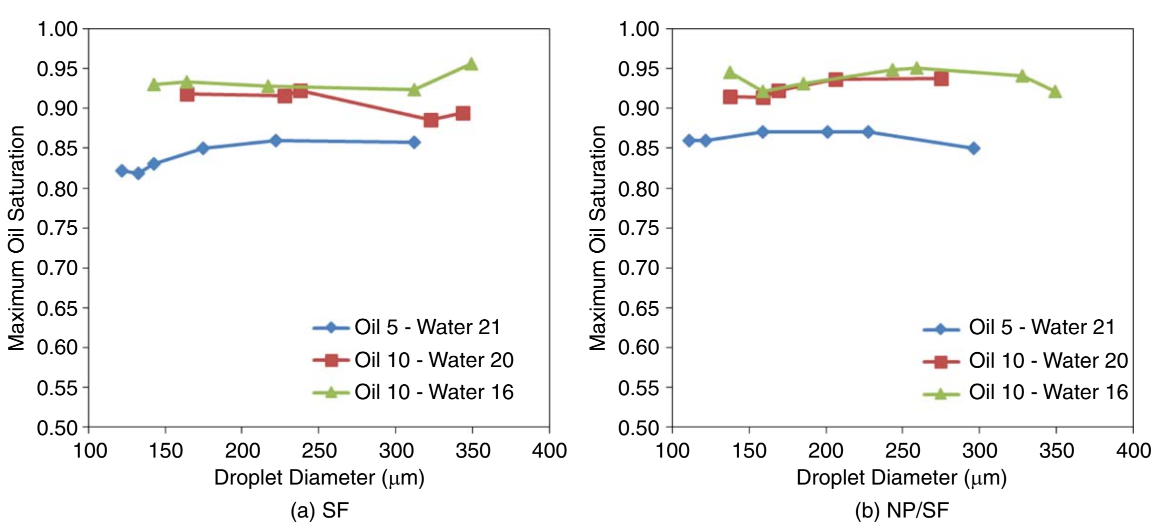

Fig. 5—Maximum oil saturation S_{om} with different oil-droplet diameters and injection ratio, when applying (a) 2 wt% Tween 40 or (b) 2 wt% NPs mixed with 0.05 wt% Tween 40 as emulsion stabilizer. Triangles represent the case for when oil flux is 10 μL/h and water flux is 16 μL/h (i.e., the fractional flow of oil is 0.385); squares represent the case when oil flux is 10 μL/h and water flux is 20 μL/h (i.e., the fractional flow of oil is 0.333); diamonds represent the case when oil flux is 5 μL/h and water flux is 21 μL/h (i.e., the fractional flow of oil is 0.192).

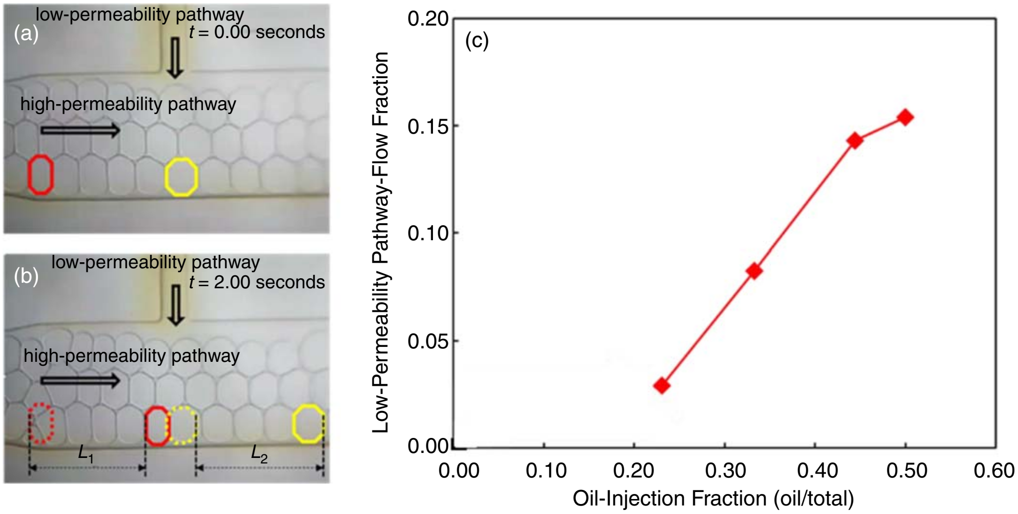

Fig. 6—(a) The image at the emergence of high- and low-permeability pathways, at time 0 seconds. The droplet surrounded by red solid lines is a droplet before emergence at this moment; the droplet surrounded by yellow solid lines is a droplet after the emergence at this moment. (b) The image at the emergence of high- and low-permeability pathways, at time of 2 seconds. The droplet surrounded by red solid lines and the droplet surrounded by yellow solid lines are the same droplets as those surrounded by red solid lines and yellow solid lines in (a), respectively. The red and yellow dashed lines indicate the positions of those two droplets at 0 seconds, respectively. L_1 and L_2 are the distances that the oil droplets were mobilized during the past 2 seconds, which are used to calculate the droplet velocities before and after emergence. (c) Plot of the relationship between low-permeability pathway flow fraction (relative to the total flow rate) and oil-injection fraction, made with the image-analysis method shown in (a) and (b).

Fig. 6b. Assuming that the velocity of the oil droplet is proportional to the total flow rate, we can calculate the flux fraction into the low-permeability pathways ($f_{\text{low-perm}}$) by the equation: $f_{\text{low-perm}} = (v_2\text{-}v_1)/v_2$. When we control the total flow rate as 30 μL/h and then change the oil-injection ratio, we can obtain the flow distribution between the low-permeability pathway flow fraction and the main channel, as shown in Fig. 6c. The stabilizer used in this set of parallel experiments is 2 wt% Tween 40. Clearly, the higher the oil-injection fraction, the more liquid will flow into low-permeability pathways. This result, together with the observation that oil blockage in the high-permeability pathway is enhanced with higher oil-injection fraction, leads to the conclusion that the oil-droplet blockage in the high-permeability pathway does have a positive effect on improving sweep efficiency.

In our experiment, it was observed that the oil ratio in the low-permeability pathway is much lower than that in high-permeability pathway, when the characteristic size of the channel cross section is controlled by the same smallest dimension (in this case, the channel depth). It has been reported that the apparent viscosity of O/W emulsion is positively related to the phase ratio of oil (Thomas and Farouq Ali 1989; Tadros 1994). Therefore, our observation indicates a thickening effect: The apparent viscosity of emulsion in the high-permeability pathway is larger than the apparent viscosity of emulsion in the low-permeability pathway. In this way, more liquid will tend to flow into the low-permeability pathway than Newtonian fluid. Because the presence of an obstruction that blocks emulsion in a high-permeability pathway usually occurs in real porous media, our observation shows a much-better potential for improving sweep efficiency and conformation control than Newtonian and shear-thinning fluids, such as polymer.

Different Packing Mode of Droplets for Two Stabilizers and Its Effect on Sweep Efficiency. In this section, we compare the blockage performance between the surfactant-stabilized emulsion (SF system) and the NP/surfactant synergistically stabilized emulsion (NP/SF system). S_{om} was averaged over the values corresponding to different droplet size and plotted against O/W injection ratio, for both SF and NP/SF systems, as shown in **Fig. 7a.** For all injection conditions, it is observed that S_{om} are always larger in the NP/SF system than in the SF system. As mentioned in the previous section, the better blockage effect in the NP/SF system than in the SF system implies more liquid into low-permeability pathways. Flow fraction in low-permeability pathways is also compared between the SF system and NP/SF system, as shown in Fig. 7b. Unfortunately, the data are not measurably different for most of the oil-injection fraction. However, the difference in droplet packing in both cases, as shown later, supports the hypothesis that an NP/SF system can better redirect liquid into low-permeability regions, and thus have a better potential in improving sweep efficiency than the SF system.

It was found from microscopic observation that the difference in S_{om} is a result of different droplet-packing densities, as seen in **Fig. 8.** Droplets stabilized by the NP/SF system experience more compression and deformation than those stabilized by SF alone, when injection rates (oil flow rate is 10 μL/h, and total water flow rate is 16 μL/h) and droplet diameters (140 ± 5 μm) are the same. For the SF system, droplets are in "point-to-point" contact with little deformation of the droplet surface. However, for the NP/SF system, droplets are squeezed and contact each other in a "lamella" fashion, in a manner very similar to that of stable dry foams (Lemlich 1968). In the SF system, relative movements between droplets were observed at all directions, whereas for the NP/SF system, all droplets were found to move together almost as a rigid body along the principal flow direction.

In general, a confined droplet tends to deform under an asymmetric pressure field around it, whereas the deformation resistance is provided by the IFT. Because the O/W IFT was found to be similar for the two systems, the deformation resistances are not much different. Thus, the difference in droplet deformation comes from the asymmetric pressure field around the droplets.

The asymmetric pressure comes from two sources: (1) hydraulic force from viscous flow field and flow, as well as (2) interactions between neighboring O/W interfaces. Flow rates for both phases are rigidly controlled to be similar in this experiment. Fig. 7b shows that although the flow fraction in the low-permeability pathway (and also in the high-permeability pathway) in the NP/SF system is larger than in the SF system, the differences are not sufficient to make a considerable difference in the main-channel flux. Furthermore, it was observed that the frequency of oil droplets flowing into the side channels is very small at all flow rates investigated, so the difference of O/W ratio in the side channel in both systems does not have a significant contribution to the pressure gradient. Therefore, hydraulic force should be approximately

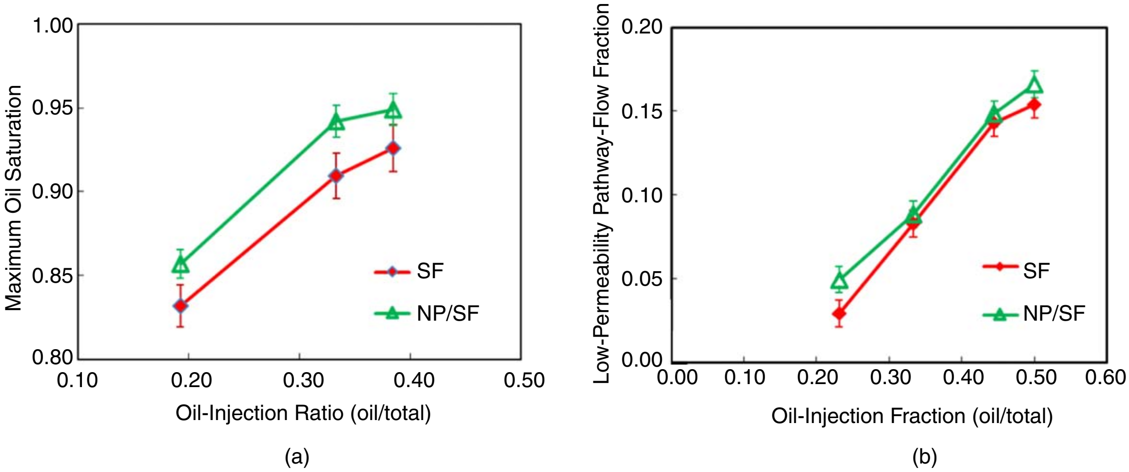

Fig. 7—(a) The comparison of maximum oil saturation for different oil-injection ratios with different emulsion stabilizer. (b) The comparison of low-permeability pathway flow fraction for different oil-injection ratios with different emulsion stabilizer. In both (a) and (b), red diamonds represent 2 wt% Tween 40 and green triangles represent 2 wt% NPs mixed with 0.05 wt% Tween 40.

the same and is not the primary reason for the different droplet-packing modes between SF and NP/SF systems.

Here, we speculate that the difference of droplet-packing arrangement upstream of the main throat is caused by the formation of an NP network in the thin aqueous liquid film between adjacent droplets (Horozov 2008; Wasan and Nikolov 2008), or even bridging induced by a monolayer of NP (Horozov and Binks 2006). NPs adsorbed on the oil–water interface can interact with other NPs, including those adsorbing on the neighboring oil–water interface, and form a network that can join two interfaces together. In this way, neighboring droplets' interfaces can be bound together when they are brought in to contact and deform under shearing force. Further research is required to determine whether surfactant also plays a role in the formation of the NP network in the thin liquid film between neighboring interfaces.

Conclusions

A microfluidic device was used to study the mechanism for sweep improvement for the emulsion-based EOR process. Emulsion with controllable droplet size, phase-injection ratio, and total flow rate was produced, and emulsion behavior in a simplified natural fracture–matrix was investigated. Important conclusions from the work are

1. A novel in-flow test of emulsion stability was used to quantitatively measure the coalescence of emulsion droplets while flowing in micron-scale porous media. Trace amounts of surfactant (0.05 wt%) with NP (2 wt%) can produce a synergistic effect to prevent droplet coalescence. The droplet stability in these systems is at least as good as that with high-concentration surfactant (2 wt%).
2. Stable emulsion droplets were found to effectively block the high-permeability pathway and improve flux through low-permeability pathways, when there is throat-like geometry in the high-permeability pathway and the droplet size is larger than the throat diameter. In this case, maximum local oil saturation immediately upstream of the throat has a weak correlation with the droplet size, which is attributed to the pressure continuity of the oil phase at that location.

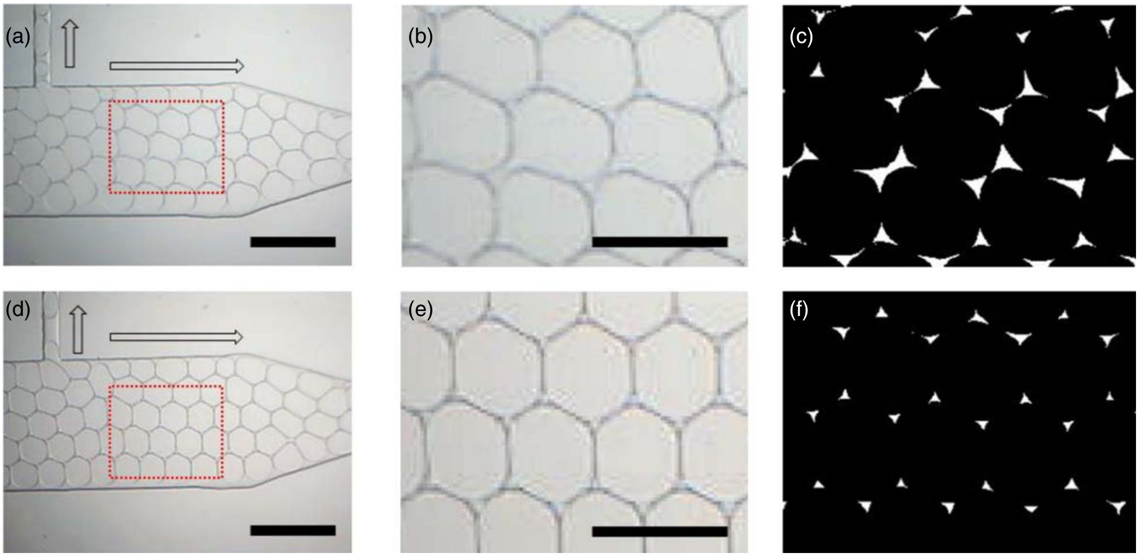

Fig. 8—Microscopic images for emulsion flow through the main channel after all divergence and before the main throat for (a)–(c) applying 2 wt% Tween 40 as emulsion stabilizer and (d)–(f) applying 2 wt% NPs mixed with 0.05 wt% Tween 40 as emulsion stabilizer. For both cases, oil-injection rate is 10 μL/h, water-injection rate is 16 μL/h, and droplet diameters are controlled at 140 ± 5 μm. (a) and (d) are origin images captured by the camera, and the scale bars represent 400 μm. (b) and (e) are local magnification of droplet-packing mode from the red squares in (a) and (d), and the scale bars represent 200 μm. (c) and (f) are processed from (b) and (e) by marking the oil phase in black and aqueous phase in white to show a clear packing mode of the droplets. Arrows in (a) and (b) indicate the flow direction.

3. The fraction of flow into the low-permeability pathways is positively related to the blockage ability of emulsion in the high-permeability pathway where a pore throat is present, which is typical in real porous media. It can be explained by the positive relationship between oil fraction and apparent viscosity in an O/W emulsion. Because oil saturation in high-permeability pathways is much larger than in low-permeability pathways, emulsion shows larger apparent viscosity in high-permeability pathways than in low-permeability pathways, which indicates that the blockage effect does have the potential to improve sweep efficiency and flood stability.
4. NP/SF stabilized emulsion can lead to a higher oil saturation before the main throat than SF-stabilized emulsion, when flow condition and droplet size are the same. The hypothesis is that NP/SF can redirect more liquid into low-permeability regions than the SF-stabilized system. It was evident by the droplet-packing images, which showed that droplets stabilized with NP/SF show closer packing mode with more deformation. This shows that an NP/surfactant synergistic system can enhance the emulsion-blockage effect compared with the surfactant as stabilizer, which can lead to a better sweep efficiency and flooding stability.

Although the injected emulsion system that contains NP/SF mixture shows a potential for improving sweep efficiency from our microscopic visualization, it is outside the scope of this work to investigate its sweep efficiency in oil recovery. In our future work, the sweep efficiency by the NP/SF emulsion system during oil recovery will be tested and quantitatively measured in a 2D micromodel.

Acknowledgments

The authors gratefully acknowledge the support from the sponsors of the Nanoparticles for Subsurface Engineering Industrial Affiliates Project at the University of Texas at Austin. The authors also thank I-Jung Kim (University of Texas at Austin), who, through many conversations, motivated us to investigate the neighboring droplets' behavior in the presence of NPs.

References

Abgrall, P. and Gué, A.-M. 2007. Lab-on-Chip Technologies: Making a Microfluidic Network and Coupling It Into a Complete Microsystem—A Review. *Journal of Micromechanics and Microengineering* **17** (5): R15–R49. http://dx.doi.org/10.1088/0960-1317/17/5/R01.

Aktas, F., Clemens, T., Castanier, L. et al. 2008. Viscous Oil Displacement via Aqueous Associative Polymers. Presented at the SPE Symposium on Improved Oil Recovery, Tulsa, 20–23 April. SPE-113264-MS. http://dx.doi.org/10.2118/113264-MS.

Alvarado, D. A. and Marsden Jr., S. S. 1979. Flow of Oil-in-Water Emulsions Through Tubes and Porous Media. *SPE J.* **19** (6): 369–377. SPE-5859-PA. http://dx.doi.org/10.2118/5859-PA.

Al-Yaseri, A. Z., Lebedev, M., Vogt, S. J. et al. 2015. Pore-Scale Analysis of Formation Damage in Bentheimer Sandstone With In-Situ NMR and Micro-Computed Tomography Experiments. *Journal of Petroleum Science and Engineering* **129:** 48–57. http://dx.doi.org/10.1016/j.petrol.2015.01.018.

Bennetzen, M. V. and Mogensen, K. 2014. Novel Applications of Nanoparticles for Future Enhanced Oil Recovery. Presented at the International Petroleum Technology Conference, Kuala Lumpur, 10–12 December. IPTC-17857-MS. http://dx.doi.org/10.2523/IPTC-17857-MS.

Bhattacharya, R. and Basu, J. K. 2013. Microscopic Dynamics of Nanoparticle Monolayers at Air-Water Interface. *J. Colloid Interface Sci.* **396:** 69–74. http://dx.doi.org/10.1016/j.jcis.2013.01.003.

Binks, B. P., Desforges, A., and Duff, D. G. 2007. Synergistic Stabilization of Emulsions by a Mixture of Surface-Active Nanoparticles and Surfactant. *Langmuir* **23** (3): 1098–1106. http://dx.doi.org/10.1021/la062510y.

Binks, B. P., Kirkland, M., and Rodrigues, J. A. 2008. Origin of Stabilization of Aqueous Foams in Nanoparticle–Surfactant Mixtures. *Soft Matter* **4:** 2373–2382. http://dx.doi.org/10.1039/B811291F.

Bizmark, N., Ioannidis, M. A., and Henneke, D. E. 2014. Irreversible Adsorption-Driven Assembly of Nanoparticles at Fluid Interfaces Revealed by a Dynamic Surface Tension Probe. *Langmuir* **30** (3): 710–717. http://dx.doi.org/10.1021/la404357j.

Boyd, J. V., Parkinson, C., and Sherman, Ph. 1972. Factors Affecting Emulsion Stability, and the HLB Concept. *Journal of Colloid and Interface Science* **41** (2): 359–370. http://dx.doi.org/10.1016/0021-9797(72)90122-1.

Chang, L-C., Tsai, J-P., Shan, H-Y. et al. 2009. Experimental Study on Imbibition Displacement Mechanisms of Two-Phase Fluid Using Micro Model. *Environmental Earth Sciences* **59:** 901–911. http://dx.doi.org/10.1007/s12665-009-0085-6.

Chevalier, Y. and Bolzinger, M-A. 2013. Emulsions Stabilized With Solid Nanoparticles: Pickering Emulsions. *Colloids and Surfaces A: Physicochemical and Engineering Aspects* **439:** 23–34. http://dx.doi.org/10.1016/j.colsurfa.2013.02.054.

Cobos, S., Carvalho, M. S., and Alvarado, V. 2009. Flow of Oil–Water Emulsions Through a Constricted Capillary. *International Journal of Multiphase Flow* **35** (6): 507–515. http://dx.doi.org/10.1016/j.ijmultiphaseflow.2009.02.018.

Conn, C. A., Ma, K., Hirasaki, G. J. et al. 2014. Visualizing Oil Displacement With Foam in a Microfluidic Device With Permeability Contrast. *Lab Chip* **14:** 3968–3977. http://dx.doi.org/10.1039/C4LC00620H.

Du, K., Glogowski, E., Emrick, T. et al. 2010. Adsorption Energy of Nano- and Microparticles at Liquid-Liquid Interfaces. *Langmuir* **26** (15): 12518–12522. http://dx.doi.org/10.1021/la100497h.

Espinoza, D. A., Caldelas, F. M., Johnston, K. P. et al. 2010. Nanoparticle-Stabilized Supercritical CO2 Foams for Potential Mobility Control Applications. Presented at the SPE Improved Oil Recovery Symposium, Tulsa, 24–28 April. SPE-129925-MS. http://dx.doi.org/10.2118/129925-MS.

Fu, Taotao, Ma, Y., Funfschilling, D. et al. 2011. Dynamics of Bubble Breakup in a Microfluidic T-Junction Divergence. *Chem. Eng. Sci.* **66** (18): 4184–4195. http://dx.doi.org/10.1016/j.ces.2011.06.003.

Garrett, E. R. 1965. Stability of Oil-in-Water Emulsions. *Journal of Pharmaceutical Sciences* **54** (11): 1557–1570. http://dx.doi.org/10.1002/jps.2600541102.

Gravesen, P., Branebjerg, J., and Søndergård Jensen, O. 1993. Microfluidics—A Review. *Journal of Micromechanics and Microengineering* **3** (4): 168. http://dx.doi.org/10.1088/0960-1317/3/4/002.

Hashemi, R., Nassar, N. N., and Almao, P. P. 2014. Nanoparticle Technology for Heavy Oil In-Situ Upgrading and Recovery Enhancement: Opportunities and Challenges. *Applied Energy* **133:** 374–387. http://dx.doi.org/10.1016/j.apenergy.2014.07.069.

Horozov, T. S. and Binks, B. P. 2006. Particle-Stabilized Emulsions: A Bilayer or a Bridging Monolayer? *Angewandte Chemie* **45** (5): 773–776. http://dx.doi.org/10.1002/anie.200503131.

Horozov, T. 2008. Foams and Foam Films Stabilized by Solid Particles. *Current Opinion in Colloid & Interface Science* **13** (3): 134–140. http://dx.doi.org/10.1016/j.cocis.2007.11.009.

Hunter, T. N., Pugh, R. J., Franks, G. V. et al. 2008. The Role of Particles in Stabilizing Foams and Emulsions. *Adv. Colloid Interface Sci.* **137** (2): 57–81. http://dx.doi.org/10.1016/j.cis.2007.07.007.

Islam, M. R. and Ali, S. M. 1989. New Scaling Criteria for Polymer, Emulsion and Foam Flooding Experiments. *J Can Pet Technol* **28** (4): 79–87. PETSOC-89-04-05. http://dx.doi.org/10.2118/85-04-05.

Karambeigi, M. S., Abbassi, R., Roayaei, E. et al. 2015. Emulsion Flooding for Enhanced Oil Recovery: Interactive Optimization of Phase Behavior, Microvisual and Core-Flood Experiments. *Journal of Industrial and Engineering Chemistry* **29:** 382–391. http://dx.doi.org/10.1016/j.jiec.2015.04.019.

Koo, J. and Kleinstreuer, C. 2003. Liquid Flow in Microchannels: Experimental Observations and Computational Analyses of Microfluidics Effects. *Journal of Micromechanics and Microengineering* **13:** 568–579. http://dx.doi.org/10.1088/0960-1317/13/5/307.

Lee, H., Lee, S. G., and Doyle, P. S. 2015. Photopatterned Oil-Reservoir Micromodels With Tailored Wetting Properties. *Lab Chip* **15** (14): 3047–3055. http://dx.doi.org/10.1039/c5lc00277j.

Lemlich, R. 1968. Adsorptive Bubble Separation Methods—Foam Fractionation and Allied Techniques. *Industrial & Engineering Chemistry* **60** (10): 16–29. http://dx.doi.org/10.1021/ie50706a005.

Ma, K., Liontas, R., Conn, C. A. et al. 2012. Visualization of Improved Sweep With Foam in Heterogeneous Porous Media Using Microfluidics. *Soft Matter* **8:** 10669–10675. http://dx.doi.org/10.1039/C2SM25833A.

Mandal, A., Samanta, A., Bera, A. et al. 2010a. Characterization of Oil-Water Emulsion and Its Use in Enhanced Oil Recovery. *Industrial & Engineering Chemistry Research* **49** (24): 12756–12761. http://dx.doi.org/10.1021/ie101589x.

Mandal, A., Samanta, A., Bera, A. et al. 2010b. Role of Oil-Water Emulsion in Enhanced Oil Recovery. Presented at the 2010 International Conference on Chemistry and Chemical Engineering (ICCCE), Kyoto, Japan, 1–3 August, 190–194. http://dx.doi.org/10.1109/ICCCENG.2010.5560393.

Martinez, A. W., Phillips, S. T., Whitesides, G. M. et al. 2010. Diagnostics for the Developing World: Microfluidic Paper-Based Analytical Devices. *Analytical Chemistry* **82** (1): 3–10. http://dx.doi.org/10.1021/ac9013989.

McAuliffe, C. D. 1973. Oil-in-Water Emulsions and Their Flow Properties in Porous Media. *J Pet Technol* **25** (6): 727–733. SPE-4369-PA. http://dx.doi.org/10.2118/4369-PA.

Mendoza, H., Thomas, S., and Ali, S. M. 1991. Effect of Injection Rate on Emulsion Flooding for a Canadian and a Venezuelan Crude Oil. Presented at the Annual Technical Meeting, Banff, Alberta, Canada, 21–24 April. PETSOC-91-26. http://dx.doi.org/10.2118/91-26.

Metin, C., Bonnecaze, R., and Nguyen, Q. 2013. The Viscosity of Silica Nanoparticle Dispersions in Permeable Media. *SPE Res Eval & Eng* **16** (3): 327–332. SPE-157056-PA. http://dx.doi.org/10.2118/157056-PA.

Nallamilli, T., Mani, E., and Basavaraj, M. G. 2014. A Model for the Prediction of Droplet Size in Pickering Emulsions Stabilized by Oppositely Charged Particles. *Langmuir* **30** (31): 9336–9345. http://dx.doi.org/10.1021/la501785y.

Nilghaz, A., Dedy, H. B., Wicaksono, D. G. et al. 2012. Flexible Microfluidic Cloth-Based Analytical Devices Using a Low-Cost Wax Patterning Technique. *Lab Chip* **12:** 209–218. http://dx.doi.org/10.1039/C1LC20764D.

Okada, M., Maeda, H., Fujii, S. et al. 2012. Formation of Pickering Emulsions Stabilized Via Interaction Between Nanoparticles Dispersed in Aqueous Phase and Polymer End Groups Dissolved in Oil Phase. *Langmuir* **28** (25): 9405–9412. http://dx.doi.org/10.1021/la3015964.

Pei, H. H., Zhang, G. C., Ge, J. J. et al. 2015. Investigation of Nanoparticle and Surfactant Stabilized Emulsion to Enhance Oil Recovery in Waterflooded Heavy Oil Reservoirs. Presented at the SPE Canada Heavy Oil Technical Conference, Calgary, 9–11 June. SPE-174488-MS. http://dx.doi.org/10.2118/174488-MS.

Pickering, S. U. 1907. CXCVI.—Emulsions. *Journal of the Chemical Society, Trans.* **91:** 2001–2021. http://dx.doi.org/10.1039/CT9079102001.

Rana, S., Yu, X., Patra, D. et al. 2012. Control of Surface Tension at Liquid-Liquid Interfaces Using Nanoparticles and Nanoparticle-Protein Complexes. *Langmuir* **28** (4): 2023–2027. http://dx.doi.org/10.1021/la204017z.

Ravera, F., Ferrari, M., Liggieri, L. et al. 2008. Liquid–Liquid Interfacial Properties of Mixed Nanoparticle–Surfactant Systems. *Colloids and Surfaces A: Physicochemical and Engineering Aspects* **323** (1–3): 99–108. http://dx.doi.org/10.1016/j.colsurfa.2007.10.017.

Rocha de Farias, M. L., de Souza, A. L., da Silveira Carvalho, M. et al. 2012. A Comparative Study of Emulsion Flooding and Other IOR Methods for Heavy Oil Fields. Presented at the SPE Latin American and Caribbean Petroleum Engineering Conference, Mexico City, 16–18 April. SPE–152290-MS. http://dx.doi.org/10.2118/152290-MS.

Romero, M. I., Carvalho, M. S., and Alvarado, V. 2011. Experiments and Network Model of Flow of Oil-Water Emulsion in Porous Media. *Phys. Rev. E* **84:** 046305. http://dx.doi.org/10.1103/PhysRevE.84.046305.

Ryles, R. G. 1988. Chemical Stability Limits of Water-Soluble Polymers Used in Oil Recovery Processes. *SPE Res Eng* **3** (1): 23–34. SPE-13585-PA. http://dx.doi.org/10.2118/13585-PA.

Sagis, L. M. C. 2011. Dynamic Properties of Interfaces in Soft Matter: Experiments and Theory. *Reviews of Modern Physics* **83:** 1367–1403. http://dx.doi.org/10.1103/RevModPhys.83.1367.

Schmitt, M., Limage, S., Grigoriev, D. O. et al. 2014. Transition From Spherical to Irregular Dispersed Phase in Water/Oil Emulsions. *Langmuir* **30** (16): 4599–4604. http://dx.doi.org/10.1021/la404766w.

Shah, R. K., Shum, H. C., Rowat, A. C. et al. 2008. Designer Emulsions Using Microfluidics. *Materials Today* **11** (4): 18–27. http://dx.doi.org/10.1016/S1369-7021(08)70053-1.

Sharma, T., Velmurugan, N., Patel, P. et al. 2015. Use of Oil-in-Water Pickering Emulsion Stabilized by Nanoparticles in Combination With Polymer Flood for Enhanced Oil Recovery. *Petroleum Science and Technology* **33** (17–18): 1595–1604. http://dx.doi.org/10.1080/10916466.2015.1079534.

Song, H. and Ismagilov, R. F. 2003. Millisecond Kinetics on a Microfluidic Chip Using Nanoliters of Reagents. *Journal of the American Chemical Society* **125** (47): 14613–14619. http://dx.doi.org/10.1021/ja0354566.

Song, W., de Haas, T. W., Fadaei, H. et al. 2014. Chip-Off-the-Old-Rock: The Study of Reservoir-Relevant Geological Processes With Real-Rock Micromodels. *Lab Chip* **14** (22): 4382–4390. http://dx.doi.org/10.1039/c4lc00608a.

Stone, H. A., Stroock, A. D., and Ajdari, A. 2004. Engineering Flows in Small Devices. *Annual Review of Fluid Mechanics* **36:** 381–411. http://dx.doi.org/10.1146/annurev.fluid.36.050802.122124.

Tadros, Th. F. 1994. Fundamental Principles of Emulsion Rheology and Their Applications. *Colloids and Surfaces A: Physicochemical and Engineering Aspects* **91:** 39–55. http://dx.doi.org/10.1016/0927-7757(93)02709-N.

Thomas, S. and Farouq Ali, S. M. 1989. Flow of Emulsions in Porous Media, and Potential for Enhanced Oil Recovery. *Journal of Petroleum Science and Engineering* **3** (1–2): 121–136. http://dx.doi.org/10.1016/0920-4105(89)90038-7.

Wan, J., Tokunaga, T. K., Tsang, C-F. et al. 1996. Improved Glass Micromodel Methods for Studies of Flow and Transport in Fractured Porous Media. *Water Resources Research* **32** (7): 1955–1964. http://dx.doi.org/10.1029/96WR00755.

Wang, X., Wang, K., Riaud, A. et al. 2014. Experimental Study of Liquid/Liquid Second-Dispersion Process in Constrictive Microchannels. *Chem. Eng. J.* **254:** 443–451. http://dx.doi.org/10.1016/j.cej.2014.05.135.

Wasan, D. and Nikolov. A. 2008. Thin Liquid Films Containing Micelles or Nanoparticles. *Current Opinion in Colloid & Interface Science* **13** (3): 128–133. http://dx.doi.org/10.1016/j.cocis.2007.11.011.

Worthen, A. J., Bryant, S. L., Huh, C. et al. 2013. Carbon Dioxide-in-Water Foams Stabilized With Nanoparticles and Surfactant Acting in Synergy. *AIChE Journal* **59** (9): 3490–3501. http://dx.doi.org/10.1002/aic.14124.

Xu, J. H., Li, S. W., Tan, J. et al. 2006. Preparation of Highly Monodisperse Droplet in a T-Junction Microfluidic Device. *AIChE Journal* **52** (9): 3005–3010. http://dx.doi.org/10.1002/aic.10924.

Xu, J-H., Zhao, H., Lan, W-J. et al. 2012. A Novel Microfluidic Approach for Monodispersed Chitosan Microspheres With Controllable Structures. *Advanced Healthcare Materials* **1** (1): 106–111. http://dx.doi.org/10.1002/adhm.201100014.

Xu, K., Tostado, C. P., Xu, J. H. et al. 2014. Direct Measurement of the Differential Pressure During Drop Formation in a Co-Flow Microfluidic Device. *Lab Chip* **14** (7): 1357–1366. http://dx.doi.org/10.1039/c3lc51222c.

Xu, K., Ge, X-H., Huang, J-P. et al. 2015a. A Region-Selective Modified Capillary Microfluidic Device for Fabricating Water–Oil Janus Droplets and Hydrophilic–Hydrophobic Anisotropic Microparticles. *RSC Adv.* **5** (58): 46981–46988. http://dx.doi.org/10.1039/C5RA05690J.

Xu, Ke, Zhu, P., Huh, C. et al. 2015b. Microfluidic Investigation of Nanoparticles' Role in Mobilizing Trapped Oil Droplets in Porous Media. *Langmuir* **31** (51): 13673–13679. http://dx.doi.org/10.1021/acs.langmuir.5b03733.

Yu, W. and Xie, H. 2012. A Review on Nanofluids: Preparation, Stability Mechanisms, and Applications. *Journal of Nanomaterials* Vol. 2012, Article ID 435873, 17 pages. http://dx.doi.org/10.1155/2012/435873.

Zhang, C., Oostrom, M., Grate, J. W. et al. 2011. Liquid CO2 Displacement of Water in a Dual-Permeability Pore Network Micromodel. *Environ. Sci. Technol.* **45** (17): 7581–7588. http://dx.doi.org/10.1021/es201858r.

Ke Xu is a graduate research assistant in the Department of Petroleum and Geosystems Engineering at the University of Texas at Austin (UTA), supervised by Matthew Balhoff. His research interests include micron-scale multiphase flow, NP behavior on liquid/liquid and liquid/gas interfaces, EOR-related pore-level experiments/theories, and application of microfluidics in other engineering areas. Xu has authored or coauthored seven technical papers. He holds an MS degree in chemical engineering from Tsinghua University, and is currently pursuing a PhD degree in petroleum engineering at UTA.

Peixi Zhu is a post-docotoral-degree researcher in the Department of Petroleum and Geosystems Engineering at UTA. His research interests include multiphase flow at multiscale, improved oil recovery, microfluidics, pore-level simulation, and NPs for subsurface applications. Zhu has contributed seven technical papers to peer-review and conference journals. He holds a PhD degree in chemical engineering from Tulane University and a BS degree in chemistry from Nanjing University, China.

Tatiana Colon is a graduate student at Texas Tech University. Previously, she worked for CooperVision Incoporated. Colon also participated in research internships at Texas Tech University in 2014 and UTA in 2015, both of which were focusing on topics in petroleum engineering. Her research interests include the following topics: EOR, fundamental processes, reservoir engineering, and NP engineering for subsurface processes. Colon holds a BS degree in chemical engineering from the Polytechnic University of Puerto Rico.

Chun Huh is a research professor in the Department of Petroleum and Geosystems Engineering at UTA. Before joining the UTA faculty in 2004, he worked as an engineering adviser at ExxonMobil Upstream Research Company in Houston. Huh holds a PhD degree from the University of Minnesota and a BS degree from Seoul National University, Korea, both in chemical engineering. He is a leading expert on surfactant- and polymer-based EOR processes. At UTA, Huh carried out research on use of NPs for a variety of upstream oil-industry applications. He is an active member of SPE. Huh received the SPE IOR Pioneer Award in 2012, and was elected an SPE Distinguished Member in 2015.

Matthew T. Balhoff is an associate professor of petroleum and geosystems engineering at UTA, where he has been since 2007. He earned a BS degree and PhD degree in chemical engineering from Louisiana State University and completed a post-doctoral-degree appointment in the Institute of Computational and Engineering Sciences at UTA in 2005. Balhoff received the 2014 SPE International Young Member Service Award and the 2012 SPE International Teaching Fellow Award. He currently serves on the SPE Research and Development Technical Section Committee.